Steel and Composite Structures, *Vol. 22, No. 6 (2016) 1261-1280*
DOI: http://dx.doi.org/10.12989/scs.2016.22.6.1261

Nonlinear vibration of laminated composite plates subjected to subsonic flow and external loads

Hamed Norouzi [1a] and Davood Younesian [*1,2]

[1] *School of Railway Engineering, Iran University of Science and Technology, Tehran 16846-13114, Iran*
[2] *Department of Mechanical Engineering, UC Berkeley, Berkeley, CA 94720-1740, USA*

(*Received June 27, 2016, Revised November 04, 2016, Accepted November 17, 2016*)

Abstract. We study chaotic motion in a nonlinear laminated composite plate under subsonic fluid flow and a simultaneous external load in this paper. We derive equations of motion of the plate using the von-Kármán's hypothesis and the Hamilton's principle. Galerkin's approach is adopted as the solution method. We then conduct a divergence analysis to obtain critical velocities of the transient flow. Melnikov's integral approach is used to find the critical parameters in which chaos takes place. Effects of different parameters including the aspect ratio, plate material and the ply angle in laminates on the critical flow speed are investigated. In a parametric study, we show that how the linear and nonlinear stiffness of the plate and the load frequency and amplitude would influence the chaotic behavior of the plate.

Keywords: composite laminated plates; vibration; subsonic flow; chaos; Melnikov's method

1. Introduction

Composite laminated plates are broadly employed in varieties of engineering applications because of their light weight and high stiffness. Automobiles, aircrafts and high speed trains are a few of the applications (Yao and Lee 2013). Complex behavior, mainly come up from the material and geometric nonlinearity is often observed in such structures. In high speed trains, external loads from vibration of the train due to the irregularity of the wheel and track surface are exerted to the body structures. The side walls as well as the roof plates are consistently subjected to the airflow. Possibility of chaotic and unpredictable oscillations is an important issue due to potential of unexpected fatigue damage in the body structure.

In the last decades, many researchers investigated the aero-elasticity field and chaotic vibrations of the nonlinear dynamical systems such as nonlinear laminated composite plates. Balachandran and Nayfeh (1990), experimentally studied the nonlinear forced response of an internally-resonant composite structure subjected to primary resonant excitations. Sing *et al.* (1990) examined nonlinear vibrations of simply supported rectangular cross-ply plates. They proposed a method of direct numerical integration of the frequency-ratio expression to analyze the nonlinear free vibration. Huang and Yang (2002) established a general solution for the free vibration of

*Corresponding author, Professor, E-mail: Younesian@iust.ac.ir; Davood.younesian@berkeley.edu
[a] Ph.D. Candidate, E-mail: h_norouzi@rail.iust.ac.ir

http://www.techno-press.org/?journal=scs&subpage=6 ISSN: 1229-9367 (Print), 1598-6233 (Online)

orthotropic rectangular thin plates for arbitrary boundary conditions. Biancolini *et al*. (2005) proposed an approximate solution for free vibrations of thin orthotropic rectangular plates. They obtained the fundamental mode of an orthotropic rectangular plate with different constraint conditions. Free vibration analysis of the orthotropic rectangular plates with variable thickness and general boundary conditions has been presented by Huang *et al*. (2005). They transformed the differential governing equations into integral equations in order to find Green's function. Korbahti and Uzal (2007) proposed an analytical solution for the vibrations of an anisotropic plate under fluid flow in a channel. Free vibration of clamped varying thickness visco-elastic rectangular plates has been studied using the Rayleigh-Ritz technique by Gupta *et al*. (2009). Xing and Liu (2009) extracted a new exact solution for free vibrations of thin orthotropic rectangular plates by introducing a novel separation of variables method. The nonlinear oscillation and chaotic behavior of a reinforced composite plate under parametric and forcing excitations were studied by Guo *et al*. (2013) using the Galerkin's method. Jiang *et al*. (2016) studied nonlinear vibrational behavior of composite laminated trapezoidal plates using finite element method (FEM). They used Hamilton's principle in order to derive the equation of motion of the plate. They examined the effects of the ply angle and the length ratio on the nonlinear vibration frequency ratios of the plates. Global bifurcations and multi-pulse chaotic dynamics of a simply supported composite piezoelectric and honeycomb sandwich rectangular plates subjected to combined parametric and transverse excitations were studied by Zhang *et al*. (Zhang *et al*. 2010, Zhang and Zhang 2012) using the extended Melnikov method. Li *et al*. (2011) examined the chaos in a two dimensional thin panel in subsonic flow and subjected to external excitation using Melnikov's method. Touzeh *et al*. (2011) employed the galerkin's approach to analyze transition from periodic to chaotic vibrations in free-edge, perfect and imperfect circular plates. Rezaei and Jahangiri (2015) employed the multiple scales method to study nonlinear and chaotic vibrations and stability of a simply supported Functionally Graded Piezoelectric (FGP) rectangular plate subjected to supersonic aerodynamic loading. Free vibration analysis of functionally graded nanocomposite triangular plates was performed by Zhang *et al*. (2012). Askari *et al*. (2015) presented a novel procedure for the nonlinear vibration analysis of curved beam by uses of non-uniform rational B-spline (NURBS) representation. Kargarnovin *et al*. (2012) examined the dynamic response of a delaminated composite beam subjected to moving oscillatory mass considering Piosson's effect, shear deformation and rotary inertia of beam.

Yao and Li (2013) examined chaotic motion of a composite laminated plate with geometric nonlinearity in subsonic flow using Melnikov's integral. Nonlinear vibration of a two-dimensional composite laminated plate in subsonic air flow has also been conducted by Yao and Li (2015). Shi *et al*. (2014) analyzed free vibrations of orthotropic rectangular Mindlin plates with general elastic boundary conditions. Younesian and Norouzi (2015) studied frequency responses of the nonlinear visco-elastic plates subjected to external forces and subsonic flow. Recently, the same authors (Younesian and Norouzi 2016) established a new method for chaos prediction in nonlinear viscoelastic plates subjected to subsonic flow and external load using extended Melnikov's integral. Song and Li (2014) employed the Finite Element method and showed that the shock waves have remarkable effects on the aero-thermal-elastic characteristics of hypersonic nonlinear laminated panels. Civalek (2013) with Akgoz (Akgoz and Civalek 2011) used the discrete singular convolution approach to study nonlinear dynamic response of rectangular laminated composite plate resting on nonlinear Winkler/Pasternak foundation.

Among all the surveyed studies in chaotic vibrations of the plates subjected to fluid flow, the plate assumed to be extended in one direction. In other words, variation of parameters in lateral

direction (*y* in our study) is assumed to be neglected. Although, this assumption can be justifiable in many applications, but it is not valid in small to moderate aspect ratios. So, this paper is to cover this gap in the literature by taking the lateral direction into account. Numerical and analytical approaches are simultaneously used to find critical flow speed, and critical parameters needed for the chaotic motions. Results in representations of critical curves, Lyapunov exponent, bifurcation diagram, time histories, state space diagrams and Poincaré section are presented and discussed in the next sections. A parametric study is then carried out to evaluate effects of different parameters on the chaotic motion of the plate.

2. Mathematical modeling

Fig. 1 shows a laminated composite plate with N layers and dimensions of a and b and thickness of h. The plate has simple supports and is subjected to subsonic air flow with the speed of U_∞ and the external load $f(x,y,t)$.

Cartesian coordinates is located at the middle surface of the plate. Without any loss of generality, the thicknesses of each layer are assumed to be equal. According to the von-Kármán's hypothesis and by ignoring the in-plane displacement in x and y directions, the strain-displacement relations in three dimensional coordinates can be expressed by

$$\varepsilon_1 = -z\frac{\partial^2 w}{\partial x^2} + \frac{1}{2}\left(\frac{\partial w}{\partial x}\right)^2, \quad \varepsilon_2 = -z\frac{\partial^2 w}{\partial y^2} + \frac{1}{2}\left(\frac{\partial w}{\partial y}\right)^2, \quad \varepsilon_6 = 2\varepsilon_{12} = -2z\frac{\partial^2 w}{\partial x \partial y} + \frac{\partial w}{\partial x}\frac{\partial w}{\partial y} \tag{1}$$

In which, ε_1, ε_2 and ε_6 are normal and shear strains and w is the mid-plane displacement in the z direction. The stresses and moment results per unit length can be defined as

$$N_i = \int_{\frac{-h}{2}}^{\frac{h}{2}} \sigma_i \, dz, \qquad M_i = \int_{\frac{-h}{2}}^{\frac{h}{2}} \sigma_i z \, dz, i = 1,2,6 \tag{2}$$

where, σ_i (i = 1, 2, 6) are the in plane stress components ($\sigma_1 = \sigma_x,\ \sigma_2 = \sigma_y,\ \sigma_6 = \tau_{xy}$).

The constitutive equations for the k^{th} layer can be represented by

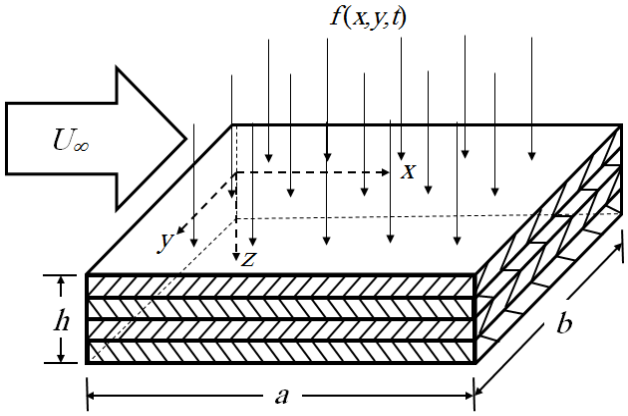

Fig. 1 Representation of a composite plate subjected to fluid flow

$$\begin{bmatrix}\sigma_1\\ \sigma_2\\ \sigma_6\end{bmatrix} = [Q]_k \begin{bmatrix}\varepsilon_1\\ \varepsilon_2\\ \varepsilon_6\end{bmatrix} \tag{3}$$

where σ_1 and σ_2 denote the normal stress and σ_6 the shear stress. Moreover, $[Q]_k$ is the reduced stiffness matrix of the k^{th} layer and can be represented as

$$[Q] = \begin{bmatrix}Q_{11} & Q_{12} & 0\\ Q_{21} & Q_{22} & 0\\ 0 & 0 & 0\end{bmatrix} \tag{4}$$

$Q_{11} = \frac{E_1}{1-\upsilon_{12}\upsilon_{21}}$, $Q_{12} = \frac{\upsilon_{12}E_1}{1-\upsilon_{12}\upsilon_{21}}$, $Q_{21} = \frac{\upsilon_{21}E_1}{1-\upsilon_{12}\upsilon_{21}}$, $Q_{22} = \frac{E_2}{1-\upsilon_{12}\upsilon_{21}}$, $Q_{66} = G$ are the stiffness coefficients, E_1, E_2 and G denote the elastic and shear module, and υ_{12}, υ_{21} are the Poisson's ratios. If the plate is assumed to be laminated composite with ply angle θ_k, then the constitutive equation equations for the k^{th} layer is transformed into the form

$$\{\sigma\}_k = [\bar{Q}]_k\{\varepsilon\}_k \tag{5}$$

in which $\bar{Q}_k = \left[H_k^{-1}\right][Q_k]\left[H_k^{-1}\right]^T$ and H_k is the transformation matrix and can be defined as (Dowell 1974)

$$H_k = \begin{bmatrix} cos^2\theta_k & sin^2\theta_k & 2sin\theta_k cos\theta_k \\ sin^2\theta_k & cos^2\theta_k & -2sin\theta_k cos\theta_k \\ -sin\theta_k cos\theta_k & sin\theta_k cos\theta_k & cos^2\theta_k - sin^2\theta_k \end{bmatrix} \tag{6}$$

The strain energy of the laminated composite plate can be obtained as

$$U = \frac{1}{2}\sum_{k=1}^{N}\int_0^a\int_0^b\int_{z_k}^{z_{k+1}} (\sigma_{1k}\varepsilon_1 + \sigma_{2k}\varepsilon_2 + \sigma_{6k}\varepsilon_6)\, dz\, dy\, dx \tag{7}$$

$$\begin{aligned} U = \frac{1}{2}\int_0^a\int_0^b \frac{1}{4}\Bigg(& A_{11}\left(\frac{\partial w}{\partial x}\right)^4 + 2(A_{12}+2A_{66})\left(\frac{\partial w}{\partial x}\right)^2\left(\frac{\partial w}{\partial y}\right)^2 + A_{22}\left(\frac{\partial w}{\partial y}\right)^4\Bigg) \\ & -B_{11}\left(\frac{\partial w}{\partial x}\right)^2\left(\frac{\partial^2 w}{\partial x^2}\right) - B_{12}\left(\left(\frac{\partial^2 w}{\partial y^2}\right)\left(\frac{\partial w}{\partial x}\right)^2 + \left(\frac{\partial^2 w}{\partial x^2}\right)\left(\frac{\partial w}{\partial y}\right)^2\right) \\ & -B_{22}\left(\frac{\partial w}{\partial y}\right)^2\left(\frac{\partial^2 w}{\partial y^2}\right) - 4B_{66}\left(\frac{\partial w}{\partial x}\right)\left(\frac{\partial w}{\partial y}\right)\left(\frac{\partial^2 w}{\partial x \partial y}\right) \\ & +D_{11}\left(\frac{\partial^2 w}{\partial x^2}\right)^2 + 2D_{12}\left(\frac{\partial^2 w}{\partial x^2}\right)\left(\frac{\partial^2 w}{\partial y^2}\right) + D_{22}\left(\frac{\partial^2 w}{\partial y^2}\right)^2 + 4D_{66}\left(\frac{\partial^2 w}{\partial x \partial y}\right)^2 dy\, dx \end{aligned} \tag{8}$$

A_{ij}, B_{ij} and D_{ij} are defined by

$$A_{ij} = \sum_{k=1}^{N}\int_{z_k}^{z_{k+1}} \bar{Q}_{ij}^{(k)} dz, \quad B_{ij} = \sum_{k=1}^{N}\int_{z_k}^{z_{k+1}} \bar{Q}_{ij}^{(k)} z dz, \quad D_{ij} = \sum_{k=1}^{N}\int_{z_k}^{z_{k+1}} \bar{Q}_{ij}^{(k)} z^2 dz \tag{9}$$

in which, z_k denotes the distance from the mid-plane to the lower surface of the k^{th} layer. The kinetic energy of the plate can be obtained as

$$T = \frac{1}{2}\int_0^a \int_0^b \left(\sum_{k=1}^{N} \rho_k h_k\right) \dot{w}^2 \, dy \, dx \tag{10}$$

where, ρ_k and h_k are the mass density and the thickness of the k^{th} layer. The virtual work done by the external forces can be expressed as

$$\delta W = \int_0^a \int_0^b (-P_a + f(x,y,t) - c\dot{w})\delta w \, dy \, dx \tag{11}$$

Here, c is the damping coefficients and $f(x,y,t) = f_0 \cos(\Omega t)$ represents the external force. Moreover, P_a represents the aerodynamics pressure due to fluid flow and can be defined according to the Bernoulli's principle as (Paidoussis 2014)

$$P_a = -\rho_\infty \left(\frac{\partial \varphi}{\partial t} + U_\infty \frac{\partial \varphi}{\partial x}\right)\Big|_{z=0} \tag{12}$$

in which, φ denotes potential function. The governing equation of φ satisfies

$$\beta^2 \varphi_{xx} + \varphi_{yy} + \varphi_{zz} = 0 \tag{13}$$

where, $\beta = \sqrt{1 - M_\infty^2}$. $M_\infty = \frac{U_\infty}{U_S}$ denotes the Mach number associated with the fluid flow. The interaction between the fluid and the plate needs to satisfy

$$\frac{\partial \varphi}{\partial z}\Big|_{z=0} = \frac{\partial w}{\partial t} + U_\infty \frac{\partial w}{\partial x} \tag{14}$$

The equation of motion of the plate can be obtained by the Hamilton's principle as (Amabili 2008)

$$\int_{t_1}^{t_2} (\delta T - \delta U)\, dt + \int_{t_1}^{t_2} \delta W \, dt = 0 \tag{15}$$

where, δT and δU are variations of kinetic and strain energy respectively. Substituting Eqs. (8), (10)-(11) in Eq. (15) and performing the variation operation in terms of w, one can obtain

$$\begin{aligned}
&\int_0^a \int_0^b \left(\sum_{k=1}^{N} \rho_k h_k\right) \ddot{w}\, \delta w \, dy \, dx \\
&+ \left\{ \frac{1}{2}\int_0^a \int_0^b -3A_{11}\left(\frac{\partial w}{\partial x}\right)^2 \left(\frac{\partial^2 w}{\partial x^2}\right) + (A_{12} + 2A_{66})\left(\left(\frac{\partial^2 w}{\partial x^2}\right)\left(\frac{\partial w}{\partial y}\right)^2\right)\right. \\
&\left. +2\left(\frac{\partial w}{\partial x}\right)\left(\frac{\partial w}{\partial y}\right)\left(\frac{\partial^2 w}{\partial x \partial y}\right) + \left(\frac{\partial^2 w}{\partial y^2}\right)\left(\frac{\partial w}{\partial x}\right)^2 - 3A_{22}\left(\frac{\partial w}{\partial y}\right)^2 \left(\frac{\partial^2 w}{\partial y^2}\right)\right.
\end{aligned} \tag{16}$$

$$-4(B_{12}-B_{66})\left(\left(\frac{\partial^2 w}{\partial x\partial y}\right)^2-\left(\frac{\partial^2 w}{\partial x^2}\right)\left(\frac{\partial^2 w}{\partial y^2}\right)\right)+2D_{11}\left(\frac{\partial^4 w}{\partial x^4}\right)$$
$$+4(D_{12}+2D_{66})\left(\frac{\partial^4 w}{\partial x^2\partial y^2}\right)+2D_{22}\left(\frac{\partial^4 w}{\partial y^4}\right)\delta w\, dy\, dx\Bigg\} \tag{16}$$

Eq. (16) forms a nonlinear partial differential equation in terms of $w(x,y,t)$. Boundary conditions of the plate can be mathematically represented by

$$B.C.\begin{cases} w=\dfrac{\partial^2 w}{\partial x^2}=0, & x=0,a \\ w=\dfrac{\partial^2 w}{\partial y^2}=0, & y=0,b \end{cases} \tag{17}$$

3. Solution methodology

Galerkin's approach is employed to transform Eq. (16) into a set of ordinary differential equations. According to the Galerkin's method, the solution of the Eq. (16) can be expressed by

$$w(x,y,t)=\sum_{n=1}^{\infty}\sum_{m=1}^{\infty}q_{mn}(t)\sin\left(\frac{m\pi x}{a}\right)\sin\left(\frac{n\pi y}{b}\right) \tag{18}$$

Younesian and Norouzi (2015) have analyzed the effect of the number of assumed modes considered in obtaining the response. It can be shown that the effect of higher modes consideration is negligible and, the first mode can appropriately reflect the nature of the response. So one can write

$$w(x,y,t)=q(t)\sin\left(\frac{\pi x}{a}\right)\sin\left(\frac{\pi y}{b}\right) \tag{19}$$

Where, the modal coefficients $q(t)$ is to be determined. Substituting Eq. (19) into Eqs. (12)-(14) the aerodynamics pressure can be determined as

$$P_a(x,y,t)=\frac{\rho_\infty U_\infty^2}{a\beta\lambda}\sin\frac{\pi\beta y}{b}\left(\left(\frac{a}{U_\infty^2}\ddot{q}-\frac{\pi^2}{a}q\right)\sin\frac{\pi x}{a}+2\frac{\pi}{U_\infty}\dot{q}\cos\frac{\pi x}{a}\right) \tag{20}$$

in which, $\lambda=\sqrt{\left(\frac{\pi}{a}\right)^2+\left(\frac{\pi}{b}\right)^2}$.

By substituting Eqs. (19)-(20) into Eq. (16) and calculating the integrals and defining dimensionless parameters

$$\zeta=a/b\,,\qquad \bar{q}=w/h\,,\qquad \omega_0=(\pi/a)^2\sqrt{D_{11}/\rho_\infty h},$$
$$\bar{t}=\omega_0 t,\bar{\Omega}=\Omega/\omega_0\,,\qquad \mu=\frac{1-\cos(\pi\beta)}{2\pi\beta^2}(a/h),\qquad \bar{m}=\sum_{k=1}^{N}\left(\frac{\rho_k}{\rho_\infty}\right)\left(\frac{h_k}{h}\right)+\frac{\mu}{\sqrt{1+\zeta^2}}, \tag{21}$$

$$\xi = \frac{1-cos(\pi\beta)}{2\pi^3\beta^2}\left(\frac{\rho_\infty U_\infty^2 a^3}{D_{11}}\right), \qquad \bar{c} = \frac{ca^2}{\pi^2}\left(\frac{1}{\sqrt{D_{11}\rho_\infty h}}\right),$$
$$\bar{D}_{12} = \frac{D_{12}}{D_{11}}, \qquad \bar{D}_{22} = \frac{D_{22}}{D_{11}}, \qquad \bar{D}_{66} = \frac{D_{66}}{D_{11}}, \qquad \bar{A}_{11} = \frac{A_{11}h^2}{D_{11}}, \tag{21}$$
$$\bar{A}_{12} = \frac{A_{12}h^2}{D_{11}}, \qquad \bar{A}_{22} = \frac{A_{22}h^2}{D_{11}}, \qquad \bar{A}_{66} = \frac{A_{66}h^2}{D_{11}}, \qquad \bar{f}_0 = \frac{a^4 f_0}{4\pi^2 D_{11}h}$$

One may arrive at the governing equation in the dimensionless form

$$\bar{m}\left(\frac{\partial^2\bar{q}}{\partial\bar{t}^2}\right) + \bar{c}\left(\frac{\partial\bar{q}}{\partial\bar{t}}\right) + \left\{1 + 2\zeta^2(\bar{D}_{12} + 2\bar{D}_{66}) + \zeta^4\bar{D}_{22} - \frac{\xi}{\sqrt{1+\xi^2}}\right\}\bar{q}$$
$$+\left\{\frac{\bar{A}_{11}}{3} - \frac{\zeta^2}{9}(\bar{A}_{12} + 2\bar{A}_{66}) + \frac{\zeta^4}{3}\bar{A}_{22}\right\}\bar{q}^3 = \bar{f}_0\cos(\bar{\Omega}\bar{t}) \tag{22}$$

Eq. (22) can also be transformed to the form

$$\left(\frac{\partial^2\bar{q}}{\partial\bar{t}^2}\right) + \psi\left(\frac{\partial\bar{q}}{\partial\bar{t}}\right) + \alpha\bar{q} + \gamma\bar{q}^3 = \eta\cos(\bar{\Omega}\bar{t}) \tag{23}$$

Here

$$\psi = \bar{c}/\bar{m}, \qquad \alpha = \left(1 + 2\zeta^2(\bar{D}_{12} + 2\bar{D}_{66}) + \zeta^4\bar{D}_{22} - \xi/\sqrt{1+\zeta^2}\right)/\bar{m},$$
$$\gamma = (\bar{A}_{11}/3 - (\zeta^2/9)(\bar{A}_{12} + 2\bar{A}_{66}) + (\zeta^4/3)\bar{A}_{22})/\bar{m}\ , \qquad \eta = \bar{f}_0/\bar{m} \tag{24}$$

Parameters δ and η are assumed to have order of magnitude ε. So, Eq. (23) can be expressed as

$$\left(\frac{\partial^2\bar{q}}{\partial\bar{t}^2}\right) + \alpha\bar{q} + \gamma\bar{q}^3 = \varepsilon\left(\eta\cos(\bar{\Omega}\bar{t}) - \psi\left(\frac{\partial\bar{q}}{\partial\bar{t}}\right)\right) \tag{25}$$

4. Divergence analysis

Stability of the plate under aerodynamic pressure is studied in this section. Obtaining the critical value of the pressure in which the behavior of the plate bifurcates is always important in the field of fluid-structure interactions. Let us, transfer the equation of motion of the plate into the well-known state-space$(x_1, x_2)^T = (q, \dot{q})^T$ formulation as

$$\begin{cases} \dot{x}_1 = x_2 \\ \dot{x}_2 = -\alpha x_1 - \gamma x_1^3 + \varepsilon(\eta\cos(\bar{\Omega}\bar{t}) - \psi x_2) \end{cases} \tag{26}$$

Eq. (26) can be interpreted as combination of an unperturbed system $\dot{X} = f(X)$ with a perturbation $\varepsilon g(X,t)$ in which

$$f(X)=\begin{pmatrix} x_2 \\ -\alpha x_1-\gamma x_1^3 \end{pmatrix},\qquad g(X,t)=\begin{pmatrix} 0 \\ \eta\cos\bar{\Omega}\bar{t}-\psi x_2 \end{pmatrix} \tag{27}$$

and, $X=(x_1,x_2)^T$. The unperturbed system associated with Eq. (26) has three stationary points as $\mathcal{S}_1:\left(-\sqrt{-\alpha/\gamma},0\right)^T$, $\mathcal{S}_2:(0,0)^T$, $\mathcal{S}_3:\left(\sqrt{-\alpha/\gamma},0\right)^T$ in which $\mathcal{S}_1$ and $\mathcal{S}_3$ are matched with centers and $\mathcal{S}_2$ is a saddle point. In order to find the critical value of the aerodynamic pressure P_a, the parameter α must be vanished and so, one can obtain the critical value of the parameter ξ as

$$\xi_{cr}=\sqrt{1+\zeta^2}(1+2\zeta^2(\bar{D}_{12}+2\bar{D}_{66})+\zeta^4\bar{D}_{22}) \tag{28}$$

Therefore, the critical speed of the flow is obtained as

$$U_\infty^{cr}=\left\{\frac{1}{U_s^2}+\left(\frac{\rho_\infty a^3}{\pi^3 D_{11}\left(\sqrt{1+\zeta^2}(1+2\zeta^2(\bar{D}_{12}+2\bar{D}_{66})+\zeta^4\bar{D}_{22})\right)}\right)\right\}^{-1/2} \tag{29}$$

It is seen that from Eq. (29) that flows with higher mass densities can reduce the critical speed of the flow. If one ignores the effect of Mach number in the aerodynamic model and parameter *b* approaches to the infinity (Approaching to a 2D model), one can obtain from Eq. (29) that $U_\infty^{cr}\to\pi^{\frac{3}{2}}\left(\frac{D}{\rho_\infty a^3}\right)^{\frac{1}{2}}$. This limiting result is quite matched with results of Yao and Li (2015) and Paidoussis (2014) which verifies the validity of the present work in this special case.

5. Melnikov's integral

Melnikov's integral provides an analytical approach to find the threshold of chaos in a nonlinear dynamical system. Eq. (26) forms a nonlinear perturbed equation which is appropriate for using Melnikov's integral. Unperturbed system associate with the Eq. (26) is represented by

$$\begin{cases} \dot{x}_1=x_2=\partial H/\partial x_2 \\ \dot{x}_2=-\alpha x_1-\gamma x_1^3=-\partial H/\partial x_1 \end{cases} \tag{30}$$

Here, $H(x_1,x_2)=\frac{x_2^2}{2}+\alpha\frac{x_1^2}{2}+\gamma\frac{x_1^4}{4}$ is Hamiltonian of the system. Homoclinic orbit associated with the system of Eq. (30) is determined as

$$q_0^{\pm}(t)=\begin{cases} \pm\sqrt{-2\alpha/\gamma}\,\mathrm{sech}\left(\sqrt{-\alpha}t\right) \\ \pm\alpha\sqrt{2/\gamma}\sinh\left(\sqrt{-\alpha}t\right)\left(1-\tanh^2\left(\sqrt{-\alpha}t\right)\right) \end{cases} \tag{31}$$

Melnikov's integral can be expressed as (Guckenheimer and Holmes 2013)

$$M(t_0)=\int_{-\infty}^{+\infty} f\left(q^0(t)\right)\wedge g(q^0(t),t+t_0)\,dt \tag{32}$$

Substituting Eqs. (27) and (31) into Eq. (32) leads to

$$M(t_0)=\int_{-\infty}^{+\infty}\alpha\sqrt{2/\gamma}\sinh(\sqrt{-\alpha}\,t)\left(1-\tanh^2\left(\sqrt{-\alpha}t\right)\right)\left(\eta\cos\Omega(t+t_0)-\psi\alpha\sqrt{2/\gamma}\sinh\left(\sqrt{-\alpha}t\right)\left(1-\tanh^2\left(\sqrt{-\alpha}t\right)\right)\right)dt \tag{33}$$

By performing the integral of Eq. (32) one can obtain Melnikov's criterion as

$$M(t_0)=\sqrt{2/\gamma}\,\eta\pi\Omega\,\mathrm{sech}\left(\pi\Omega/2\sqrt{-\alpha}\right)\sin(\Omega t_0)-\frac{4(-\alpha)^{3/2}\psi}{3\gamma} \tag{34}$$

Melnikov's technique states that chaos in a nonlinear system occurs if the expression of $M(t_0)$ vanishes. Setting Eq. (34) to zero gives the critical parameter ratio as

$$\left(\frac{\eta}{\psi}\right)_{cr}=\frac{2\sqrt{2}(-\alpha)^{3/2}}{3\pi\Omega\gamma^{1/2}}\cosh\left(\frac{\pi\Omega}{2\sqrt{-\alpha}}\right) \tag{35}$$

Where, $(\eta/\psi)_{cr}$ is the critical value of (η/ψ) in which the dynamical system experiences chaotic oscillations. For the values of $(\eta/\psi)>(\eta/\psi)_{cr}$ the plate can vibrate chaotically but, for the values of $(\eta/\psi)<(\eta/\psi)_{cr}$ the plate has periodic oscillations.

6. Results and discussions

Critical flow speed curves and the thresholds of the chaos are analyzed and discussed in this section. Results have been obtained for the system with parameters listed in Table 1.

Fig. 2 represents the homoclinic orbit of the unperturbed system of Eq. (30). The consequent pressure from the air flow acting on the midpoint of the plate is plotted in the time domain for the

Table 1 Parameters used in the analysis of the laminated composite plate (Yao and Li 2015)

Parameter	Value
E_1 (Pa)	1.41e11
E_2 (Pa)	9.1e9
v_{12}	0.3
v_{21}	0.0194
G (Pa)	7.2e9
ρ (Kg/m^3)	1600
H (m)	0.0025
ρ_∞ (Kg/m^3)	1.29
U_∞ (Km/h)	350
a (m)	1.0
b (m)	0.8

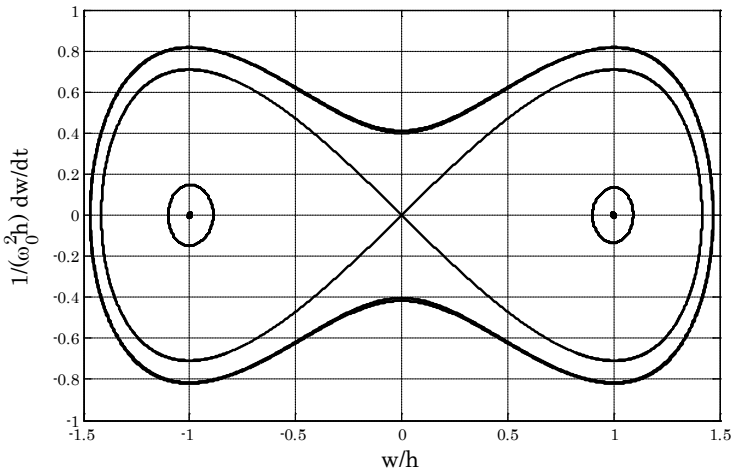

Fig. 2 Homoclinic orbit of the unperturbed system associated with the Eq. (26)

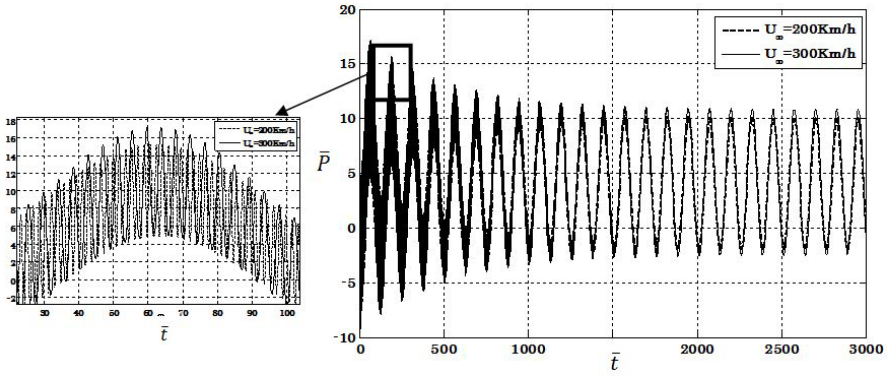

Fig. 3 Time history of the aerodynamic pressure acting on the mid-point of the plate for two different flow speeds lower than the critical speed

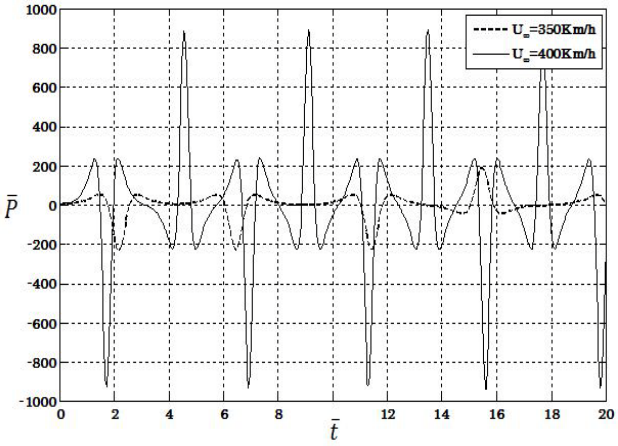

Fig. 4 Time history of the aerodynamic pressure acting on the mid-point of the plate for two different flow speeds upper than the critical speed

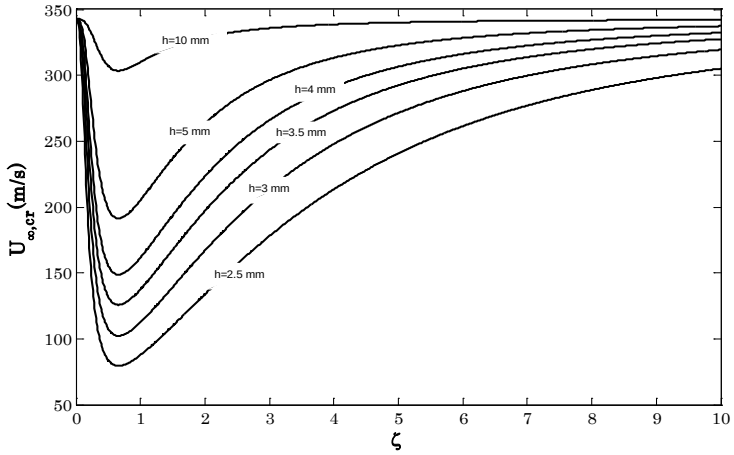

Fig. 5 Critical speed of the flow versus aspect ratio ζ for different plate thicknesses

flow speeds lower and upper than the critical speed in Figs. 3 and 4 respectively. It can be seen that increasing the flow speed in low speed regime has not significant effect on the maximum pressure. In other hand, in high-speed regime, any excessive speed can extremely influence the maximum pressure of the flow.

Fig. 5 illustrates the critical value of the flow speed versus the aspect ratio of the laminated composite plate. It is seen that the critical speed increases as the thickness of the plate increases. It is also found that there is a critical value for the aspect ratio (~ 0.7) called demerit ratio in which the critical flow speed takes its minimum value. This is an important result since this value is almost independent to the thickness value.

Fig. 6 represents the critical flow speed in terms of the aspect ratio for different types of the plate material. It is seen that the critical speed of the composite plate is something between the steel and aluminum plate in practical range of the aspect ratios (Larger than 1.0). This is also an important outcome since we can understand that the composite plate is performing well in comparison with the Aluminum.

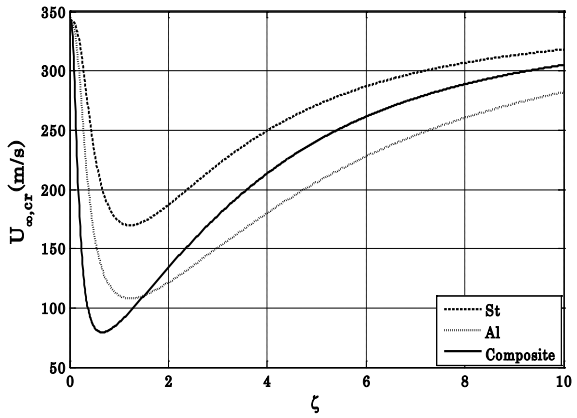

Fig. 6 Critical speed of the flow versus aspect ratio ζ for different materials

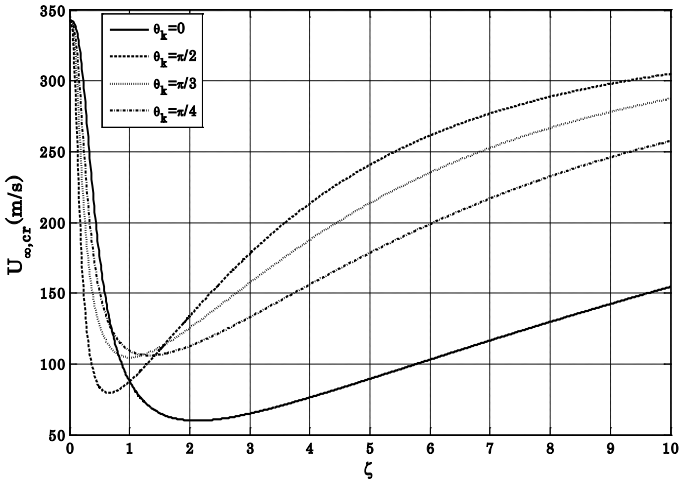

Fig. 7 Critical speed of the flow versus aspect ratio ζ for different ply angles

The critical speeds of the laminated composite plate for various ply angles have been plotted in Fig. 7. The figure shows that the critical speed of the laminated composite plate with $\theta_k = \pi/2$ has good performance and stability for $\zeta > \zeta_{\text{Dem}}$ in fluid flows with respect to the ply angles of 0, $\pi/3$, $\pi/4$. Moreover, for $\zeta < \zeta_{\text{Dem}}$, composite plates with ply angle $\theta_k = 0$ has greater critical speed.

Figs. 8 and 9 illustrate the transition curve associated with the threshold of chaotic behavior of the plate versus its linear stiffness. These figures are provided using the Melnikov's integral introduced in Eq. (32). Fig. 8 focuses on the various forcing frequencies. It is seen that forces with higher frequencies can lead to chaos occurrence in smaller amplitudes. Furthermore, the system with higher linear stiffness has larger threshold of chaos. This threshold has been demonstrated in terms of the nonlinear stiffness of the plate in Fig. 9. It is seen that increasing of the nonlinear term can lead to decrease onset of the chaos.

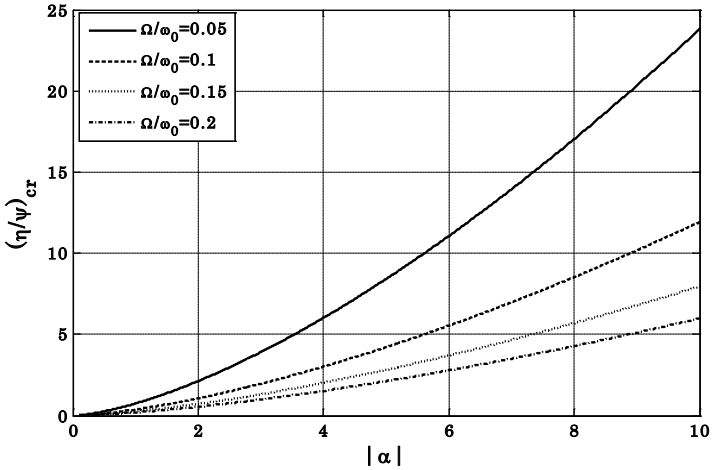

Fig. 8 **C**haos threshold versus α for different forcing frequencies

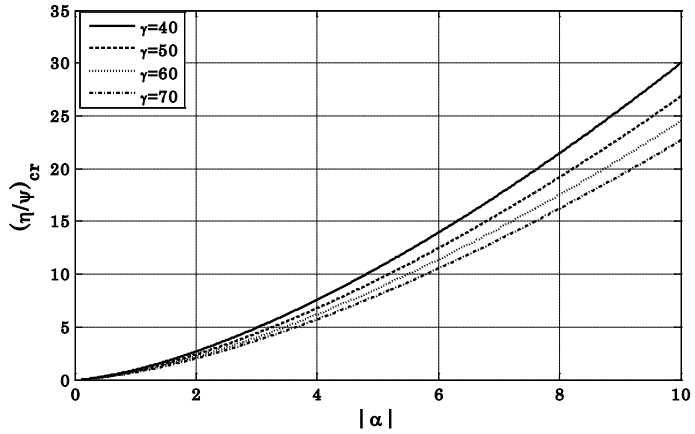

Fig. 9 Chaos threshold versus α for different values of nonlinear coefficient

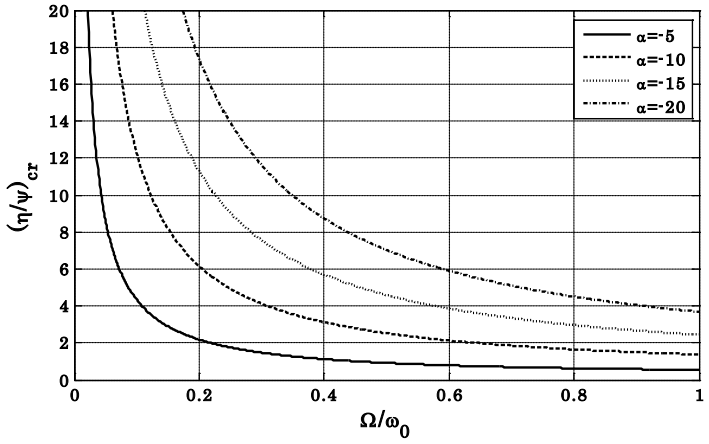

Fig. 10 Critical curve of the chaos threshold versus Ω/ω_0 for different values of linear stiffness

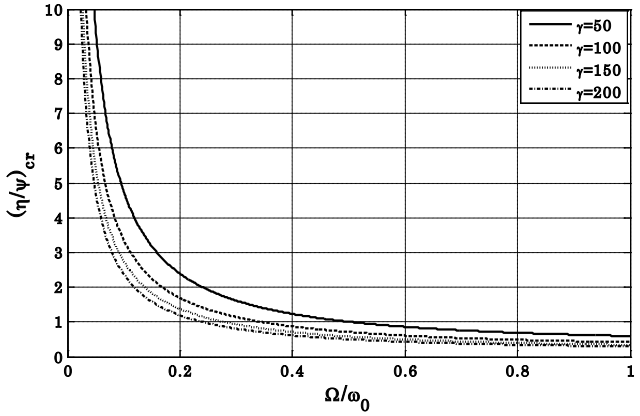

Fig. 11 Chaos threshold versus Ω for different values of the nonlinear stiffness

By increasing the frequency of the external force when the linear and nonlinear stiffness coefficients are preserved, threshold of chaos gets dropped off. This fact can be seen in the Figs. 10 and 11. It can be observed from Eqs. (21)-(22) when the flow speed increases, the parameter α takes lower magnitudes and the plate can behave chaotically even in low amplitudes of external loading. Fig. 11 also shows variations of the threshold of the chaos in terms of the linear and nonlinear stiffness of the system. Increasing the frequency of the external load leads to decrease the chaos threshold similar to increasing the nonlinear stiffness term. This trend is also seen in Fig. 12 and 13. By increasing the linear coefficient, the system can be put away from chaotic oscillations.

Chaos occurrence in the nonlinear dynamical systems can be numerically predicted via the Lyapunov exponent and bifurcation diagrams. These numerical graphs can validate the analytical Melnikov's method described before. Variation of the Lyapunov exponent for the system of Eq. (26) is plotted for $\alpha = -4, \gamma = 60, \Omega = \pi$ in Fig. 14. Corresponding bifurcation diagram is illustrated in Fig. 15 for $= -4, \gamma = 60, \Omega = \pi$. Chaos occurrence again is seen for the values of η/ψ around 6.0. Back to the analytical results given by Melnikov's integral method presented

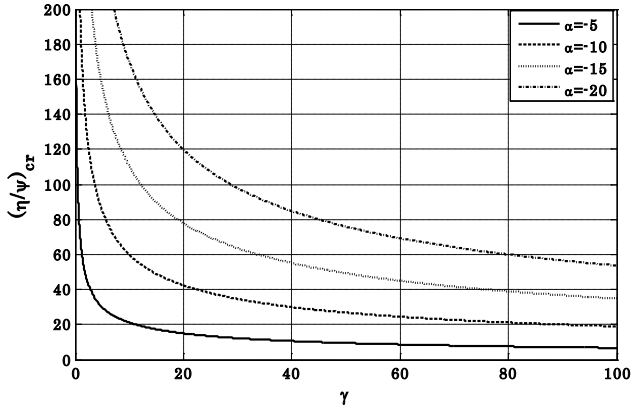

Fig. 12 Chaos threshold versus γ for different values of the linear stiffness

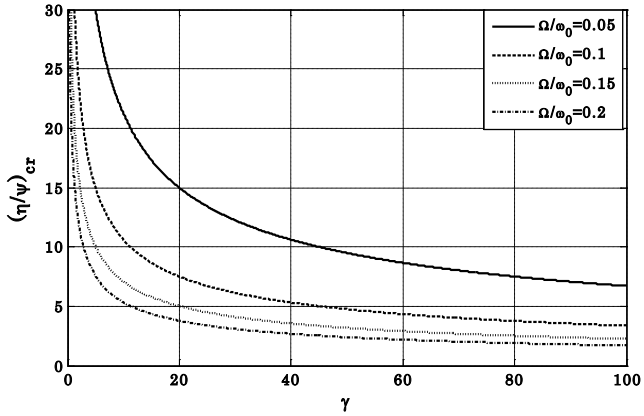

Fig. 13 Chaos threshold versus γ for different values of the forcing frequencies

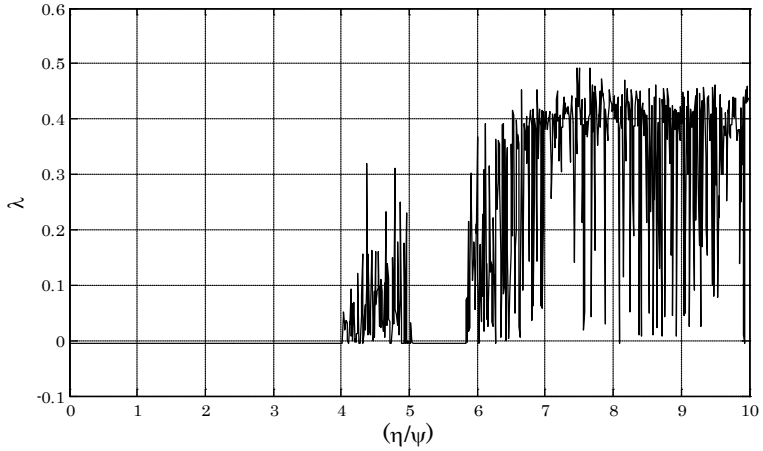

Fig. 14 Lyapunov exponent of the system of Eq. (26) for $\alpha = -4, \gamma = 60, \Omega = \pi$

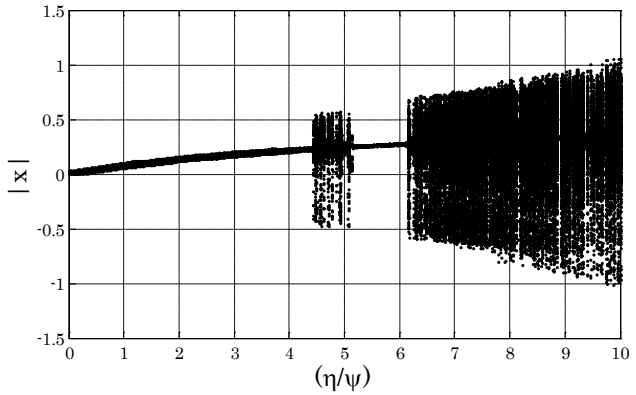

Fig. 15 Bifurcation diagram of the system of Eq. (26) for $\alpha = -4, \gamma = 60, \Omega = \pi$

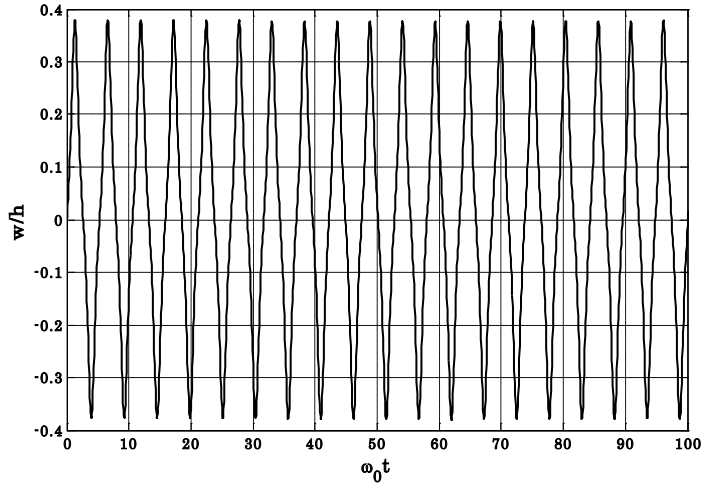

Fig. 16 Time response of the system for $(\eta/\psi) < (\eta/\psi)_{cr}$

in Fig. 9, by picking $|\alpha| = 4$, similar to these two different methods we get the same result of $\eta/\delta \approx 6$. This multiple matching between the critical values for three different approaches numerically verifies validity of the results.

The time response and state-space diagram of the midpoint of the plate is demonstrated for the conditions of $(\eta/\psi) < (\eta/\psi)_{cr}$ and $(\eta/\psi) > (\eta/\psi)_{cr}$ in Figs. 16-19. Figs. 16 and 17 show that the plate behaves periodically in the condition of $(\eta/\psi) < (\eta/\psi)_{cr}$ while it performs as a chaotic system for $(\eta/\psi) > (\eta/\psi)_{cr}$. Dense orbits can be noticeably seen in the state-space in Fig. 19.

A Poincaré cut for the nonlinear system is observed in Fig. 20 for $(\eta/\psi) > (\eta/\psi)_{cr}$. This Poincaré section shows chaotic behavior of the plate very well in the condition of high-speed flow.

After the chaos recognition in a dynamical system, in many cases the chaotic motion should be controlled. This could be mainly achieved by passive algorithms via adjusting material damping or

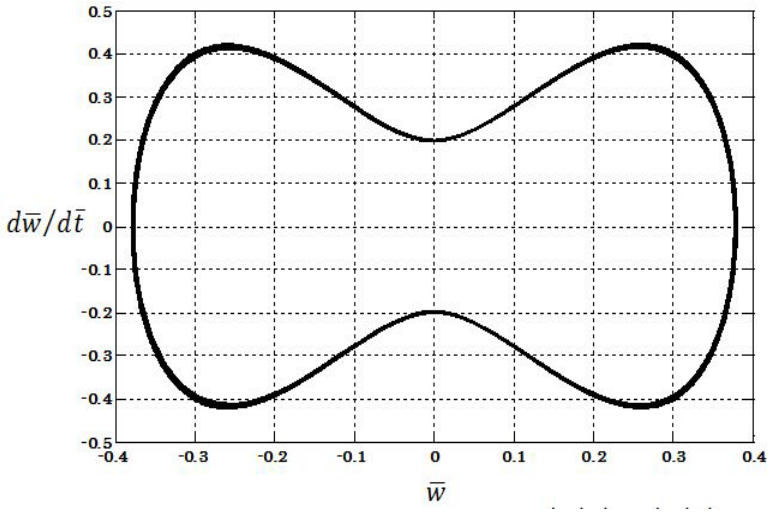

Fig. 17 State-space diagram of the system for $(\eta/\psi) < (\eta/\psi)_{cr}$

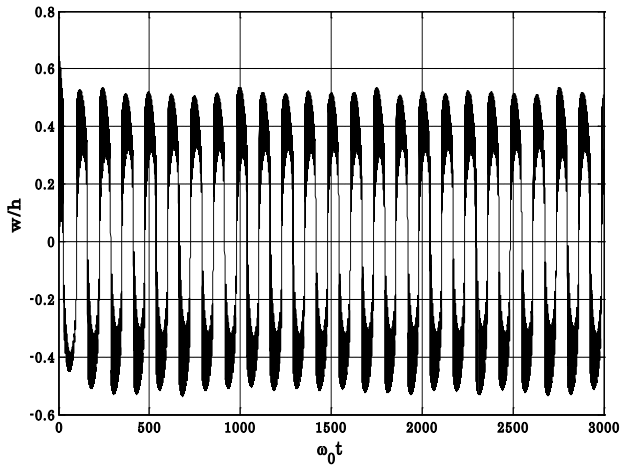

Fig. 18 Time evolution of the system for $(\eta/\psi) > (\eta/\psi)_{cr}$

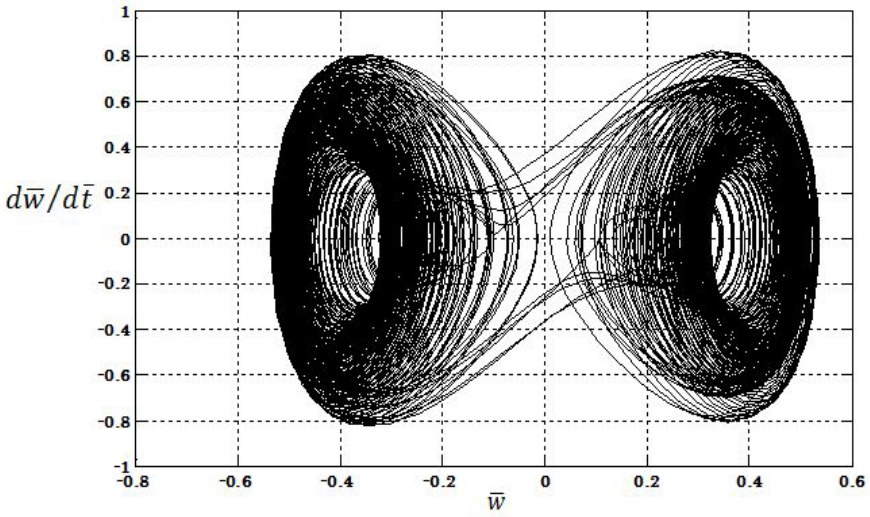

Fig. 19 State-space diagram of the system for $(\eta/\psi) > (\eta/\psi)_{cr}$

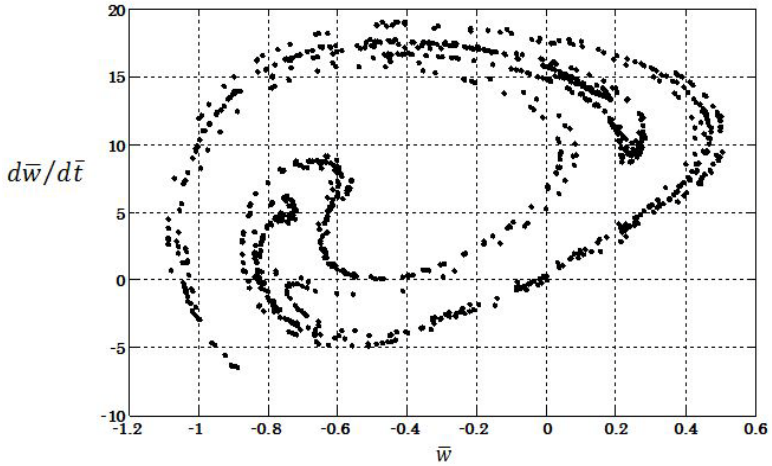

Fig. 20 Poincaré section of the system for $(\eta/\psi) > (\eta/\psi)_{cr}$

geometrical aspects or by active approaches via additional control forces. Comprehensive studies have been presented in the literature in this research line but for this particular case Norouzi and Younesian (2016) evaluated performance of different strategies in control of chaos for the pales subjected to subsonic flows.

7. Conclusions

Chaotic oscillation of a nonlinear laminated composite plate under subsonic air flow was studied when it was subjected to an external harmonic load. Dimensionless form of the equations of motion were derived by use of the Hamilton's principle and solved using the Galerkin's

approach. Melnikov's integral was analytically assembled and calculated for the system. A criterion to predict chaos was developed in terms of the ratio of the external loading amplitude to the damping coefficient. A divergence analysis was conducted to find the critical speed curves versus the plate aspect ratio. In a parametric study, effects of the plate thickness, material and the ply angles on the critical flow speeds were investigated. The followings are the main outcomes of this study:

- Neglecting the variations in "*y*" direction may result in remarkable surplus estimation for the critical speed.
- There is a specific aspect ratio called demerit ratio (0.7 in our case), in which the plate experiences a minimum value for the critical flow speed. This demerit ratio is not dependent on the plate thickness.
- Beyond the demerit ratio, critical speed increases by increasing the aspect ratio.
- Composite plates have lower critical speeds than the steel but higher than the Aluminum in practical range of the aspect ratios.
- Laminated composite plates with ply angle of 0 and $\pi/2$ have optimal performance in terms of chaos occurrence respectively within and beyond the demerit ratio.
- Linear rigidity of the plate enhances the chaos threshold while the nonlinear stiffness, loading frequency and amplitude of the external force reduce it.
- In high-speed regime, even small excessive flow speed can extremely influence the maximum pressure of the flow while in low-speed regime it has not significant effect.
- Lyapunov exponent and bifurcation diagrams numerically validated the results obtained from the developed Melinkov's integral.

Acknowledgments

The research described in this paper was financially supported by the National High-speed Train Mega-project at research office, Iran University of Science and Technology. Authors acknowledge the support received for fulfillment of this research.

References

Akgoz, B. and Civalek, O. (2011), "Nonlinear vibration analysis of laminated plates resting on nonlinear two-parameters elastic foundations", *Steel Compos. Struct., Int. J.*, **11**(5), 403-421.

Amabili, M. (2008), *Nonlinear Vibrations and Stability of Shells and Plates*, Cambridge University Press, London, UK.

Askari, H., Esmailzadeh, E. and Barari, A. (2015), "A unified approach for nonlinear vibration analysis of curved structures using non-uniform rational B-spline representation", *J. Sound Vib.*, **353**, 292-307.

Balachandran, B. and Nayfeh, A.H. (1990), "Nonlinear oscillations of a harmonically excited composite structure", *Compos. Struct.*, **16**(4), 323-339.

Biancolini, M.E., Brutti, C. and Reccia, L. (2005), "Approximate solution for free vibrations of thin orthotropic rectangular plates", *J. Sound Vib.*, **228**(1), 321-344.

Civalek, O. (2013), "Nonlinear dynamic response of laminated plates resting on nonlinear elastic foundations by the discrete singular convolution-differential quadrature coupled approaches", *Compos. Part B: Eng.*, **50**, 171-179.

Dowell, E.H. (1974), *Aeroelasticity of Plates and Shells*, Springer, Berlin, Germany.

Guckenheimer, J. and Holmes, P.J. (2013), *Nonlinear Oscillations, Dynamical Systems, and Bifurcations of Vector Fields*, Springer, Berlin, Germany.

Guo, X.Y., Zhang, W., Zhao, M.H. and He, Y.C. (2013), "A new kind of energy transfer from high frequency mode to low frequency mode in a composite laminated plate", *Acta Mech.*, **224**(12), 2937-2953.

Gupta, A.K., Khanna, A. and Gupta, D.V. (2009), "Free vibration of clamped visco-elastic rectangular plate having bi-direction exponentially thickness variations", *J. Theor. Appl. Mech.*, **47**(2), 457-471.

Huang, Y. and Yang, X.J. (2002), "General analytical solution of transverse vibration for orthotropic rectangular thin plates", *J. Mar. Sci. Appl.*, **1**(2), 78-82.

Huang, M., Ma, X.Q., Sakiyama, T., Matuda, H. and Morita, C. (2005), "Free vibration analysis of orthotropic rectangular plates with variable thickness and general boundary conditions", *J. Sound Vib.*, **228**(4), 931-955.

Jiang, G., Li, F. and Li, X. (2016), "Nonlinear vibration analysis of composite laminated trapezoidal plates", *Steel Compos. Struct., Int. J.*, **21**(2), 395-409.

Kargarnovin, M.H., Ahmadian, M.T. and Jafari-Talookolaei, R.A. (2012), "Dynamics of a delaminated Timoshenko beam subjected to a moving oscillatory mass", *Mech. Based Des. Struct. Machines*, **40**(2), 218-240.

Korbahti, B. and Uzal, E. (2007), "Vibrations of an anisotropic plate under fluid flow in a channel", *J. Vib. Control*, **13**(8), 1191-1204.

Li, P., Yang, Y. and Zhang, M. (2011), "Melnikov's method for chaos of a two dimensional thin panel in subsonic flow with external excitation", *Mech. Res. Commun.*, **38**(7), 524-528.

Nettles, A.T. (1994), *Basic Mechanics of Laminated Composite Plates*, Marshal Space Flight Center MSFC, AL, USA.

Norouzi, H. and Younesian, D. (2016), "Chaos control for the plates subjected to subsonic flow", *Regul. Chao. Dyn.*, **21**(4), 437-454.

Paidoussis, M.P. (2014), *Fluid-Structure Interactions*: *Slender Structures and Axial Flow*, Academic Press, Oxford, UK.

Rezaei, M. and Jahangiri, R. (2015), "Nonlinear and chaotic vibration and stability analysis of an aero-elastic piezoelectric FG plate under parametric and primary excitations", *J. Sound Vib.*, **344**, 277-296.

Shi, D., Zhaung, Z. and Zhang, T. (2014), "Free vibration analysis of orthotropic rectangular Mindlin plates with general elastic boundary conditions", Proceeding of Inter-Noise Conference; Institute of Noise Control Engineering, Vol. 249, No. 7

Sing, G., Kanaka Raju, K., Venkateswara Rao, G. and Iyengar N.G.R. (1990), "Nonlinear vibrations of simply supported rectangular cross-ply plates", *J. Sound Vib.*, **142**(2), 213-226.

Song, Z.G. and Li, F.M. (2014), "Aerothermoelastic analysis of nonlinear composite laminated panel with aerodynamic heating in hypersonic flow", *Compos. Part B: Eng.*, **56**, 830-839.

Touzeh, C., Thomas, O. and Amabili, M. (2011), "Transition to chaotic vibrations for harmonically forced perfect and imperfect circular plates", *Int. J. Nonlinear Mech.*, **46**(1), 234-246.

Xing, Y.F. and Liu, B. (2009), "New exact solutions for free vibrations of thin orthotropic rectangular plates", *Compos. Struct.*, **89**(4), 567-574.

Yao, G. and Li, F.M. (2013), "Chaotic motion of a composite laminated plate with geometric nonlinearity in subsonic flow", *Int. J. Non-Linear Mech.*, **50**, 81-90.

Yao, G. and Li, F.M. (2015), "Nonlinear vibration of a two dimensional composite laminated plate in subsonic air flow", *J. Vib. Control*, **21**(4), 662-669.

Younesian, D. and Norouzi, H. (2015), "Frequency analysis of the nonlinear viscoelastic plates subjected to subsonic flow and external loads", *Thin-Wall. Struct.*, **92**, 65-75.

Younesian, D. and Norouzi, H. (2016), "Chaos prediction in nonlinear viscoelastic plates subjected to subsonic flow and external load using extended Melnikov's method", *Nonlinear Dyn.*, **84**(3), 1163-1179.

Zhang, J.H. and Zhang, W. (2012), "Multi-pulse chaotic dynamics of non-autonomous nonlinear system for a honeycomb sandwich plate", *Acta Mech.*, **223**(5), 1047-1066.

Zhang, W., Zhang, J.H., Yao, M.H. and Yao, Z.G. (2010), "Multi-pulse chaotic dynamics of non-autonomous nonlinear system for a laminated composite piezoelectric rectangular plate", *Acta Mech.*,

211(1-2), 23-47.
Zhang, L.W., Lei, Z.X. and Liew, K.M. (2015), “Free vibration analysis of functionally graded carbon nanotube-reinforced composite triangular plates using the FSDT and element-free IMLS-Ritz method”, *Compos*. *Struct*., **120**, 189-199.

CC